JGR Biogeosciences

RESEARCH ARTICLE
10.1029/2024JG008338

Midday Depression of Photosynthesis in *Spartina alterniflora* in a Virginia Salt Marsh

H. M. Mast[1] and **X. Yang**[1]

[1]Department of Environmental Sciences, University of Virginia, Charlottesville, VA, USA

Key Points:

- We observe ubiquitous midday depression of photosynthesis in *Spartina alterniflora*, a C_4 salt marsh grass, during four growing seasons
- Lower high tides and warmer air temperatures were associated with a more severe midday depression of photosynthesis
- These results highlight the need to understand the complexities of *S. alterniflora* responses to environmental stress at short time scales

Supporting Information:

Supporting Information may be found in the online version of this article.

Correspondence to:

H. M. Mast and X. Yang,
hm4vd@virginia.edu;
xiyang@virginia.edu

Citation:

Mast, H. M., & Yang, X. (2025). Midday depression of photosynthesis in *Spartina alterniflora* in a Virginia salt marsh. *Journal of Geophysical Research: Biogeosciences*, *130*, e2024JG008338. https://doi.org/10.1029/2024JG008338

Received 27 JUN 2024
Accepted 17 AUG 2025

Author Contributions:

Conceptualization: H. M. Mast, X. Yang
Formal analysis: H. M. Mast
Funding acquisition: X. Yang
Investigation: H. M. Mast
Methodology: H. M. Mast, X. Yang
Project administration: X. Yang
Supervision: X. Yang
Visualization: H. M. Mast
Writing – original draft: H. M. Mast
Writing – review & editing: H. M. Mast, X. Yang

Abstract Salt marshes sequester a disproportionately large amount of carbon dioxide (CO_2) from the atmosphere through high rates of photosynthesis and carbon burial. Climate change could potentially alter this carbon sink, particularly the response of vegetation to environmental stressors that can decrease photosynthesis. Midday depression of gross primary production (GPP), characterized by a decline in photosynthesis during midday, has been documented in multiple ecosystems as a response to drought, high temperatures, and other stressors linked to climate change. Yet, midday depression has not been thoroughly investigated in salt marsh ecosystems. Here, we show that the midday depression of GPP in a *Spartina alterniflora* salt marsh on the Eastern Shore of Virginia was ubiquitous and occurred on 76% of the 283 days studied during the 2019–2022 growing seasons. GPP was estimated from eddy covariance measurements with flux partitioning. Using random forest, we found that the daily maximum tidal height and air temperature were the strongest predictors of midday depression of GPP, with lower high tides and warmer temperatures associated with more severe depression. This result suggests midday depression occurs when GPP decreases in the afternoon in response to salinity and water stress. To our knowledge, this is the first examination of midday depression of photosynthesis in *S. alterniflora* at the ecosystem scale. Our results highlight the potential of climate change to increase midday depression of photosynthesis and ultimately weaken the salt marsh carbon sink.

Plain Language Summary Photosynthesis of salt marshes removes a significant amount of carbon dioxide (CO_2) from the atmosphere and can help mitigate climate change. However, it is unclear how salt marsh photosynthesis will respond to numerous climate change-driven vegetation stressors in the coming decades. Midday depression of photosynthesis, where the rate of photosynthesis declines during midday, has been increasingly observed in a range of ecosystems in response to drought, heat waves, and other vegetation stressors. In this study, we developed an approach to quantify the daily occurrence and severity of midday depression of photosynthesis in a salt marsh on the Eastern Shore of Virginia. We observed midday depression during 76% of the 283 summertime days examined in the study from 2019 to 2022. The depression was more severe on days with lower high tides and warmer air temperatures. Both conditions can lead to salinity and water stress for vegetation. We suspect this stress causes a decrease in photosynthesis in the afternoon hours. These results suggest that climate change may exacerbate midday depression of photosynthesis.

1. Introduction

Despite their limited global spatial coverage, salt marshes play a disproportionately large role in the global carbon cycle. High rates of photosynthesis and carbon storage per unit area make salt marshes one of the most powerful natural carbon sinks, removing 49.6 ± 9.4 Tg CO_2 yr^{-1} from the atmosphere and storing carbon at densities up to 10 times greater than terrestrial ecosystems (Duarte et al., 2013; Lovelock & Reef, 2020; Mcleod et al., 2011; Rosentreter et al., 2023). The conservation and restoration of salt marshes could potentially help mitigate the impacts of climate change by sequestering atmospheric CO_2 on millennial time scales and serve as a nature-based solution (Duarte et al., 2013; Griscom et al., 2017; Nellemann & Corcoran, 2009; Rosentreter et al., 2023).

However, a wide range of climate change stressors threaten the salt marsh carbon cycle and its potential as a nature-based solution. Photosynthesis under future climate change scenarios is particularly uncertain, with numerous vegetation stressors likely to increase in the coming decades. While the effects of rising temperatures on vegetation productivity are generally well studied, the impact of temperature on *Spartina alterniflora* (*S. alterniflora*), a C_4 salt marsh cordgrass, at the ecosystem scale remains unclear. From warming experiments and leaf-level studies, *S. alterniflora* is known to increase photosynthesis with rising temperature up to its optimum temperature range of 30°C–35°C, beyond which assimilation decreases (Charles & Dukes, 2009; Ge

et al., 2014; Giurgevich & Dunn, 1979; Kathilankal et al., 2011). Ecosystem-scale studies utilizing eddy covariance (EC) flux towers have associated greater marsh CO_2 uptake with warmer temperatures and longer growing seasons at the seasonal scale; however, cooler temperatures may enhance gross primary production (GPP) over short time scales (Forbrich et al., 2018; Knox et al., 2018). Kirwan et al. (2009) attributed a latitudinal gradient in *S. alterniflora* productivity to temperature and length of the growing season and modeled a marsh productivity increase of 10%–40% with 2°C–4°C of warming over the next century. Rising temperatures will also increase the vapor pressure deficit (VPD), which can induce stomata closure and reduce photosynthesis (Grossiord et al., 2020; Knox et al., 2018).

Altered precipitation patterns, more frequent and severe droughts, and longer tidal flooding caused by sea level rise are also expected to affect marsh productivity in the coming decades by changing marsh soil moisture and salinity (O'Donnell et al., 2024; Poppe & Rybczyk, 2021). Precipitation is an important variable regulating marsh productivity because it can reduce soil salinity (De Leeuw et al., 1990; Dunton et al., 2001; Forbrich et al., 2018). In situ precipitation enhances vegetation productivity, especially in the marsh interior (Hawman et al., 2024). The productivity of vegetation along creekbanks is more sensitive to increased river discharge driven by inland precipitation (Biçe et al., 2023; Hawman et al., 2024; Więski & Pennings, 2014). However, extreme precipitation events have been linked to marsh dieback events due to sediment waterlogging (Rolando et al., 2023; Stagg et al., 2021). Marsh soil desiccation and hypersalinity during droughts have also been attributed to numerous marsh dieback events in the southeastern United States and reduced photosynthesis (Alber et al., 2008; Hughes et al., 2012; H. Li et al., 2022; McKee et al., 2004; Rolando et al., 2023; Russell et al., 2023). Longer tidal flooding due to sea level rise can provide nutrients and help alleviate hypersaline soils that accumulate during drought or low tide periods, but excessive flooding can limit oxygen availability and lead to sulfide buildup (Lamers et al., 2013).

While many studies have examined the response of *S. alterniflora* productivity to environmental stress, gaps remain in our understanding of the subdaily responses in the natural environment. Vegetation is known to respond to stress at different time scales, and diurnal patterns of GPP, or photosynthesis at the ecosystem scale, can be highly variable throughout the day (X. Li et al., 2021; Lin et al., 2019; Paul-Limoges et al., 2018). GPP can be estimated using EC by partitioning the photosynthetic component of the measured net ecosystem exchange (NEE) flux of CO_2, which was utilized in this study. Understanding the diurnal variations in GPP can disentangle photosynthesis controls that may be obscured at longer temporal scales.

Midday depression of GPP, when plants have a lower photosynthetic rate in the afternoon than in the morning at the same sunlight intensity, is one subdaily response of vegetation to environmental stress observed in various plant functional types (Lin et al., 2019; D. Q. Xu & Shen, 1996). Lin et al. (2019) examined the diurnal hysteresis of GPP at 82 EC flux tower sites and found that most plant functional types exhibited some degree of midday depression; however, grasslands and croplands demonstrated less hysteresis (no wetland sites were included in the data set). Multiple tower-based EC flux studies have attributed midday depression of GPP to stomata closure during warm afternoons with high VPD and low soil moisture, especially during droughts and heat waves (Lasslop et al., 2010; Lin et al., 2019; Qiu et al., 2020; Wilson et al., 2003; H. Xu et al., 2020). Geostationary satellites have also observed midday depression of GPP at large spatial scales during droughts and heat waves (Khan et al., 2022; X. Li et al., 2021, 2023). Midday depression has been reported in C_3, C_4, and CAM vegetation, but it is considered less common in C_4 and CAM plants that are generally more adaptive to temperature and water stress (Bräutigam & Gowik, 2016; Lara & Andreo, 2011; Lin et al., 2019; Pardo & VanBuren, 2021; H. Xu et al., 2020). To what extent *S. alterniflora* salt marshes show midday depression of GPP is unclear.

This study examines the diurnal patterns of GPP in an *S. alterniflora* salt marsh in Virginia. Our primary research questions include the following: How often and to what extent does midday depression of photosynthesis occur? What environmental factors may drive the severity of the depression? To quantify the frequency and severity of midday depression, we fit photosynthesis-irradiance curves to GPP flux data and calculate a percent depression as the reduction in afternoon photosynthesis relative to the morning for a given amount of incoming sunlight. This quantitative approach allowed us to examine the daily variability of midday depression and potential environmental drivers more closely. We then use a random forest model to examine the environmental drivers of the midday depression. To our knowledge, this is the first study to report and investigate midday depression of photosynthesis in a C_4 salt marsh grass at the ecosystem scale. Our results challenge conventional assumptions of

diurnal patterns of C_4 vegetation photosynthesis and highlight the need to better understand how individual species may respond to climate change stressors at the subdaily scale.

2. Methods

2.1. Site Description

The study site was in an intertidal salt marsh dominated by *S. alterniflora* (salt marsh cordgrass; also referred to as *Sporobolus alterniflorus* (Peterson et al., 2014a, 2014b)) within the Virginia Coast Reserve Long-Term Ecological Research site (VCR-LTER) on the Eastern Shore of Virginia (AmeriFlux ID US-VFP; 37°24′N, 75°50′W). The marsh is on the Atlantic Ocean side of the Delmarva Peninsula, facing shallow coastal lagoons backed by barrier islands. The area has a relative rising sea level trend of 5.75 mm/yr (NOAA, 2022a). No major rivers drain into the area. The flux tower is located 2 km from the shoreline and 85 m from a major creek edge. The marsh is dominated by the intermediate form of *S. alterniflora*, with an average height of 0.6 m. The area has a semidiurnal tidal cycle with two daily high and low tides and a tidal amplitude of ∼1.3 m. Tidal flooding duration, when the tide is above the marsh platform, averages 2 hr for a single high tide event, but it can be longer during spring tides or shorter during neap tides.

2.2. Eddy Covariance and Environmental Data

We collected EC measurements of the NEE flux of CO_2 from May through September in the 2019 to 2022 growing seasons. A sonic anemometer (Gill Windmaster) and an open-path infrared gas analyzer (LI-COR 7500DS) were mounted on the tower 3 m above the marsh canopy to measure 3-dimensional wind speed and CO_2 and H_2O mixing ratios at 10 Hz. The EC data were processed in EddyPro (version 7.0.9, LI-COR (2020)) and custom MATLAB scripts to align with FLUXNET protocols (Pastorello et al., 2020). NEE fluxes were calculated as the covariance between the mean deviations of vertical wind speed and gas molar density over a 30-min block average. A double wind rotation was performed to account for any sonic anemometer misalignment (Wilczak et al., 2001). Molar densities were processed with a spike removal (Vickers & Mahrt, 1997). Fluxes were filtered with a u-star threshold estimation based on a moving point test (Papale et al., 2006). Air density fluctuations were compensated with Webb, Pearman, and Leuning correction terms added to the fluxes (Webb et al., 1980). High- and low-pass frequency corrections were applied to the flux as described in Moncrieff et al. (1997, 2005), respectively.

Stationarity and turbulence tests were used to flag fluxes with a 0-1-2 quality control score, with 0 being the highest quality flux (Foken et al., 2005). Only fluxes with a quality flag of 0 were used in subsequent analysis. To account for precipitation, high humidity, and sediment obstructing the sensor light paths, NEE fluxes with a CO_2 signal strength of less than 80% were filtered from the data set. GPP was partitioned from the NEE flux using a nighttime approach in the REddyProc software package (Reichstein et al., 2005; Wutzler et al., 2018). We did not use any gap-filled flux data in the analysis presented in this paper. All fluxes measured when the tide was above the marsh mud platform were removed from the data set to avoid the effects of water limiting marsh-air gas exchange on the observed diurnal pattern. This tidal filtering removed 16% of fluxes from the total data set. To examine the diurnal patterns of CO_2 fluxes during the growing season, NEE, GPP, and respiration fluxes were averaged by hour of day from May to September for each study year and plotted against the average hourly photosynthetically active radiation (PAR).

Air temperature was measured 3.4 m above the marsh canopy and averaged over the 30-min flux interval. VPD was calculated as the difference between the actual water vapor pressure and its saturation pressure for a given air temperature, as described in the EddyPro software instruction manual (LI-COR, 2020). PAR (PQS1, Kipp & Zonen) was measured at 1-min intervals and averaged over the 30-min flux interval. Mean higher high water (MHHW) tidal data were retrieved from NOAA's nearby Wachapreague tidal station (NOAA, 2022a). A water depth sensor (CTD-Diver, Van Essen) was installed next to the flux tower in 2021 and 2022 to determine when the tide was flooding the marsh vegetation. The in situ sensor data were then used to calibrate the NOAA tidal data to determine when the tide moved above or below the marsh platform during the entire study period.

To compare environmental conditions during the study period with a longer-term average, the mean daily air temperature, total precipitation, and mean daily peak and minimum tidal height for each study year were compared to the 2009–2018 average during May–September. Due to the unavailability of continuous data from

the flux tower before 2019, data from the U.S. Climate Reference Network in Cape Charles, VA, and NOAA tidal station were utilized for all years in the comparative analysis (Diamond et al., 2013; NOAA, 2022b).

2.3. Photosynthesis-Irradiance Curves and Quantifying Midday Depression of GPP

To quantify the severity of midday depression of photosynthesis at daily and seasonal scales, we fit morning and afternoon photosynthesis-irradiance (PI) curves to GPP and PAR data from the morning (6:00–10:00 local standard time (LST)) and the afternoon (14:00–18:00 LST) using Equation 1:

$$\mathrm{GPP} = \frac{P_{\max} \times \mathrm{PAR}}{\mathrm{KI} + \mathrm{PAR}} \tag{1}$$

where GPP is the measured half-hour GPP flux, $P_{\max}$ is the curve coefficient representing the maximum rate of photosynthesis, PAR is the measured PAR, and KI is the curve coefficient representing the half-saturation constant (the irradiance at which half of $P_{\max}$ is reached). Daily PI curves were fit to a single morning or afternoon of GPP and PAR data. Seasonal PI curves were fit to morning or afternoon GPP and PAR data that were pooled for each study year. PI curves with fewer than five fitting data points, a root mean square error greater than 2.5 μmol m^{-2} s^{-1}, or an R^2 less than 0.5 were removed from subsequent analysis.

We calculated the depression of GPP as the normalized percent difference in the area under paired morning and afternoon PI curves for single days and each study year with Equation 2 as follows:

$$\text{Depression of GPP} = \frac{\mathrm{Area}_{\mathrm{afternoon}} - \mathrm{Area}_{\mathrm{morning}}}{\mathrm{Area}_{\mathrm{morning}}} \times 100 \tag{2}$$

A negative percent depression indicates that GPP is reduced in the afternoon compared to the morning for a given amount of PAR. For each study year, we tested the statistical difference between pooled daily morning and afternoon PI curve GPP values at three PAR conditions with two-sample *t*-tests at a 5% significance level. For example, all daily morning curve GPP values at 500 μmol photons m^{-2} s^{-1} from 2019 were pooled and compared to the pooled afternoon curves GPP values in the same study year and at the same PAR condition. A *t*-test was done at three PAR conditions of 500, 1,000, and 1,500 μmol photons m^{-2} s^{-1} and 4 study years, for a total of 12 tests.

Of the 612 days during the study period, 54 days had an instrument malfunction or a site power outage. Of the remaining days with data, and after tidal filtering, 439 mornings and 424 afternoons had at least five GPP and PAR data pairs to fit a PI curve. The $R^2 < 0.5$ filter flagged 49 (11%) morning and 39 (9%) afternoon daily-scale PI curves. The RMSE > 2.5 μmol m^{-2} s^{-1} filter flagged 18 (4%) morning and 18 (4%) afternoon daily-scale PI curves. The R^2 and RMSE filters together removed 75 days from subsequent analysis. No seasonal morning or afternoon PI curves were flagged by the R^2 or RMSE filters. The distribution of the R^2 and RMSE of the morning and afternoon daily-scale PI curves can be found in Figure S1 in Supporting Information S1. In total, 283 days had high-quality morning and afternoon PI curves that could be used to calculate a daily-scale depression of GPP and input into the random forest model.

Violin plots of the daily depressions of GPP, binned by the hour of the daytime peak high tide, were generated to examine relationships between the timing of high tides and the depression. The violins were plotted based on the time of the peak tide on the day of the depression calculation—the GPP flux at the time of the peak tide was not included in PI curve fitting if the tide had flooded the marsh platform.

2.4. Random Forest

To identify potential environmental drivers of midday depression, we trained a random forest model to predict the depression of GPP on a daily scale using daily total PAR, average air temperature between 6:00 and 18:00 LST, maximum VPD, total precipitation on the previous day, and maximum and minimum tidal heights as model predictors. Total precipitation on the previous day was used because EC fluxes measured during precipitation events were filtered from the data set and thus many days with precipitation did not have enough data to fit PI curves. Maximum and minimum tidal height were defined as the peak and the trough of the MHHW measured

between 6:00 and 18:00 LST at NOAA's Wachapreague tidal station. Cross-referencing with a water table depth sensor at the flux tower determined the MHHW was ∼0 m when the tide was at the same height as the marsh platform. The model was trained using MATLAB's TreeBagger package with 1,000 regression trees and sampled with replacement on a 0.7 in-bag training fraction (MATLAB, 2022). The model's R^2 was calculated as the squared correlation between the model's predicted depression and the out-of-bag depression calculated with Equation 2. The out-of-bag permuted predictor delta error was used to represent predictor importance. To visualize the marginal impact of each predictor on the predicted depression, partial dependence plots were generated using MATLAB's partial dependence function.

3. Results

3.1. Environmental Conditions

During the study period (2019–2022), our study site had a mean growing season temperature of 24.7°C, peak tides of 0.20 m, and 391 mm of precipitation (Table 1 in Supporting Information S1). These environmental conditions vary across years. 2019 and 2020 had higher mean peak tides of 0.23 and 0.21 m, respectively. 2021 had a much lower mean peak tide of 0.15 m, due to particularly low tides in July and August, and was the only year with a lower mean peak tide than the 2009–2018 average of 0.16 m. The warmest study year was 2019 with a mean air temperature of 25.5°C, which was well above the 2009–2018 mean of 24.6°C. 2019 also had a higher average maximum VPD than the other study years. The coolest year was 2020, with an average air temperature of 24.2°C. 2021 and 2022 had mean air temperatures of 24.5°C and 24.6°C, respectively. All 4 study years received less precipitation than the 2009–2018 average of 520 mm. The wettest study year was 2021 with 452 mm of rain. 2019 had a particularly dry summer with only 333 mm of rain. Although 2020 and 2022 had a total precipitation of 374 and 406 mm, respectively, both years were particularly dry in the midsummer months.

3.2. Diurnal Patterns of CO_2 Fluxes

The average summertime diurnal pattern of NEE was skewed toward morning hours in all study years (Figure 1a). NEE peaked (was the most negative) at 10:00 LST in 2019, 2021, and 2022, while 2020 peaked slightly later at 11:00 LST. NEE decreased by 15.0% (2019), 6.4% (2020), 16.7% (2021), and 19.6% (2022) between 10:00 and 14:00 LST.

For GPP, the diurnal patterns in 2019, 2021, and 2022 were markedly skewed to the morning hours, with peaks in GPP at 10:00 LST, 2 hours before PAR peaked at noon (Figure 1b). GPP was the largest in 2020, which was the only year that GPP peaked at the same time as PAR. However, GPP in 2020 was depressed in the afternoon compared to the morning, 12:00–14:00 LST GPP was less than 10:00–12:00 LST GPP. Respiration also showed asymmetrical diurnal patterns and gradually increased from the midmorning to midafternoon hours in all study years (Figure 1c).

3.3. Photosynthesis-Irradiance (PI) Curves and Depression of GPP

The seasonal PI curves and calculated percent depression of GPP for each study year suggested chronic summertime midday depression (Figures 2a–2d). Depressions of GPP were −18% and −17% in 2021 and 2022, respectively. In 2019 and 2020, there were milder seasonal depressions of −13% and −9%, respectively. The daily-scale midday depression of GPP ranged from −55% to +79% and approached more positive percent depressions (i.e., higher afternoon GPP) toward the end of the growing seasons in September (Figures 3a and 3b). Of the 283 days studied, 215 days exhibited a negative percent depression of GPP, and the depression averaged −11% across all study days. When averaged using 10-day moving windows, only 2020 had any period of positive depression between June and August.

An example of PI curve fitting at the daily scale is presented for 12 July 2021, in Figure S2 in Supporting Information S1. The P_{max} coefficients from the daily-scale PI curves also demonstrate the midday depression of GPP, with P_{max} values from the afternoon curves shifted to smaller maximum photosynthesis rates than those from the morning curves (Figure S3 in Supporting Information S1). The distribution of KI from the daily-scale PI curves did not show a marked difference between morning and afternoon, indicating no difference in the point at which the vegetation reached light saturation (Figure S3 in Supporting Information S1). The daily morning and afternoon PI

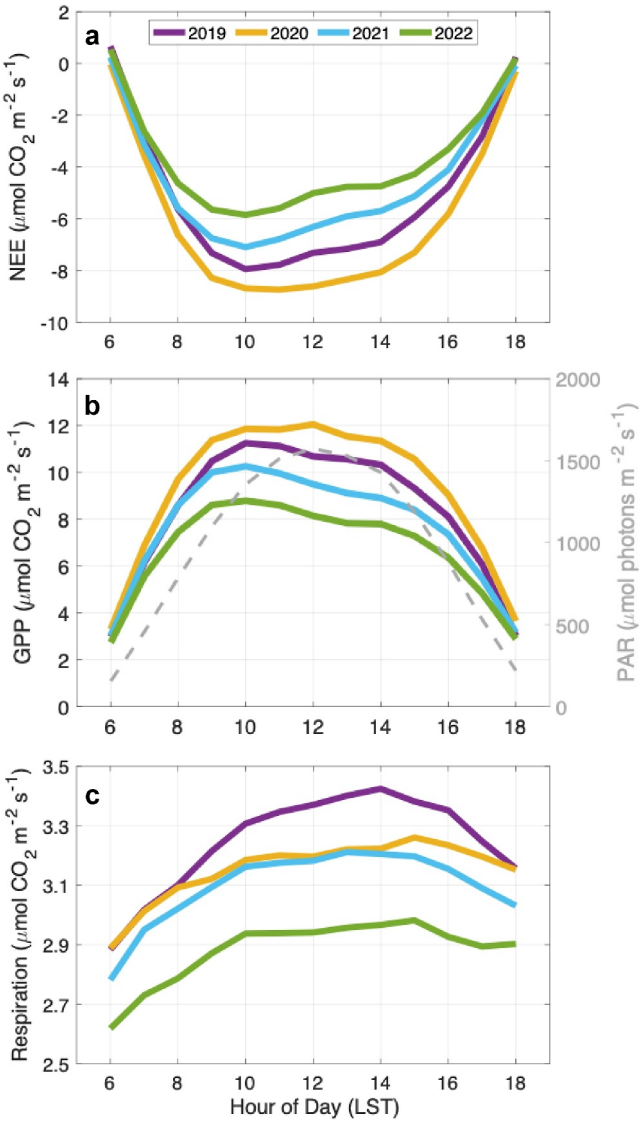

Figure 1. Diurnal patterns of (a) net ecosystem exchange (NEE) of CO_2, (b) gross primary production (GPP), and (c) respiration. The fluxes were averaged by hours of day from May to September for each study year. Each colored line represents a single study year's average. The dashed gray line in the GPP panel is the diurnal pattern of photosynthetically active radiation averaged across all study years.

curves were statistically different within each study year for the three tested PAR conditions (*t*-test, *p*-value <0.05, Table 2 in Supporting Information S1).

3.4. Environmental Drivers of Midday Depression of GPP

The random forest model identified maximum daily tidal height and average daily temperature as the most important predictors of the daily depression of GPP (Figure 4). Daily total PAR and maximum VPD were also identified as moderate predictors, while daily minimum tidal height and precipitation were found to be minimally important. The root mean square error and R^2 between the model's predicted and observed midday depression of GPP were 13% and 0.61, respectively, indicating that the model explained 61% of the variability in the daily-scale depression of GPP. Partial dependence plots in Figure 5 illustrate the marginal relationships between the model sensitivity and each input predictor. Generally, daily maximum and minimum tidal height showed a positive relationship with the model sensitivity—as these predictors increased, the depression sensitivity became less negative, leading to a less severe midday depression (Figures 5a and 5e). In contrast, the model sensitivity and predicted depression became more negative as air temperature, PAR, or VPD increased (Figures 5b–5d). The severity of depression was insensitive to precipitation on the previous day (Figure 5f).

When binned by the hour of daytime high tide, the percent depression of GPP was more severe (more negative) on days when the high tide occurred in the late afternoon (Figure 6). The most negative mean percent depressions of GPP occurred on days with a peak high tide at 16:00 LST (mean: −24.4% and median: −24.5%). Decreasing water availability throughout the day, leading to decreased photosynthesis in the afternoon, may explain this result. Combined with the maximum tidal height being the strongest predictor in the random forest model, water availability and soil salinity are likely important controls of the severity of the depression of GPP.

4. Discussion

Understanding the responses of vegetation to climate change-driven stressors at subdaily time scales is critical to forecasting photosynthetic CO_2 uptake under future climate scenarios. Further, subdaily observations are necessary to constrain larger-scale models that often rely on single-overpass satellite observations. In this study, we examine the diurnal patterns of photosynthesis in an *S. alterniflora* salt marsh and observe the ubiquitous midday depression of GPP during four growing seasons at daily and seasonal time scales. The severity of the depression varied between years and within seasons in response to environmental drivers, predominantly tidal height and air temperature.

The midday depression of GPP is likely caused by high salinity and low water availability during periods of lower tides and warmer temperatures. Despite being a salt-tolerant species, the optimal range of salinity for specific salt marsh species can be narrow (Odum, 1988; Poppe & Rybczyk, 2021). Hypersaline and dry soils can build up beyond a stress threshold when warm temperatures enhance evaporation from the marsh surface and during neap tide conditions when tidal flooding depth is reduced and shorter in duration (Shen et al., 2018; Xin et al., 2013, 2017; X. Xu et al., 2024). Further, the marsh in this study is not near a significant river mouth that could provide a freshwater input to relieve low soil moisture and high salinity, which may explain why precipitation was not a more important model predictor. Although we did not have frequent enough soil moisture and salinity observations to use it as a random forest model predictor, we measured salinities over 40 parts per thousand during periods of low tidal flooding and warm temperatures (data not shown), which exceeded the salinity stress

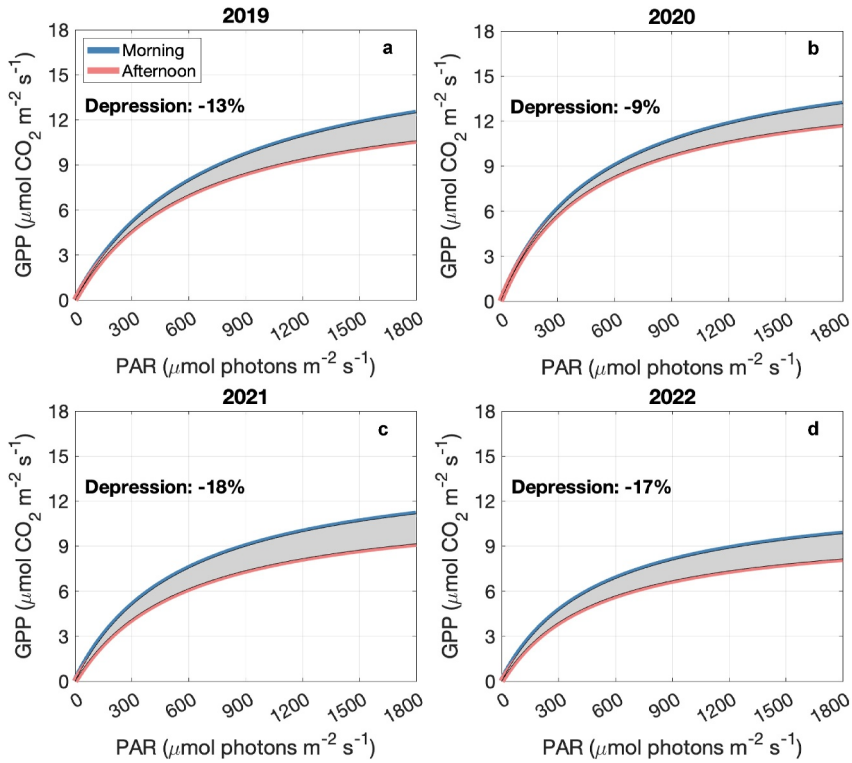

Figure 2. Morning (blue) and afternoon (pink) photosynthesis-irradiance curves for each study year. The curves were fitt with half-hourly gross primary production (GPP) and photosynthetically active radiation (PAR) data for each study year. The shaded area represents the difference in the area under each paired morning and afternoon curve. The depression percentage was calculated with Equation 2, where a negative percentage indicates a reduced GPP for a given PAR level in the afternoon relative to the morning.

threshold of 30–35 parts per thousand identified in previous work (Kathilankal et al., 2011; Maricle, Cobos, & Campbell, 2007; Pearcy & Ustin, 1984).

High salinity and low soil moisture can reduce photosynthesis through multiple mechanisms. Salinity and soil moisture are important controls of stomatal conductance (Hessini et al., 2021; Hwang & Morris, 1994; Maricle & Lee, 2006; Maricle, Cobos, & Campbell, 2007). High salinity and low soil moisture raise the osmotic potential of

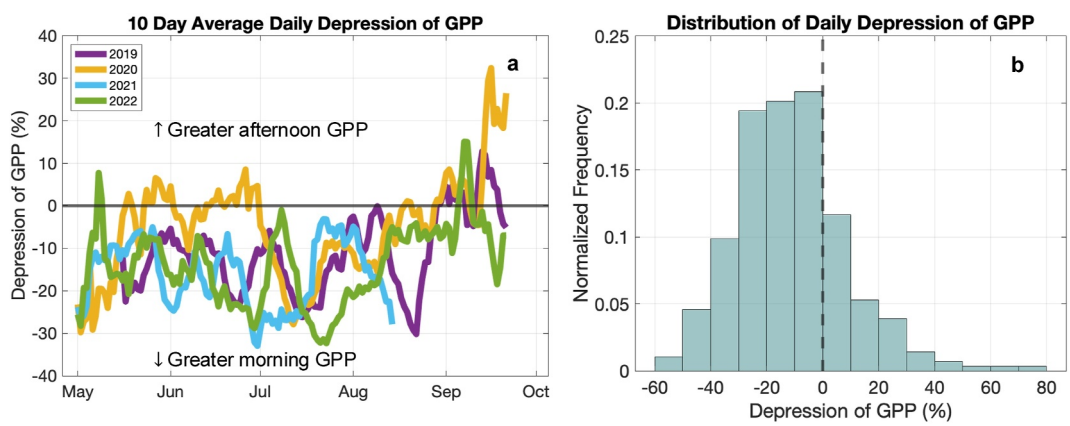

Figure 3. (a) Time series of daily percent depression of gross primary production (GPP) averaged over 10-day moving windows. (b) The distribution of daily percent depression of GPP. Any values below the 0 line in panel (a) or to the left of the dashed 0 line in panel (b) indicate observations where midday depression of GPP occurs.

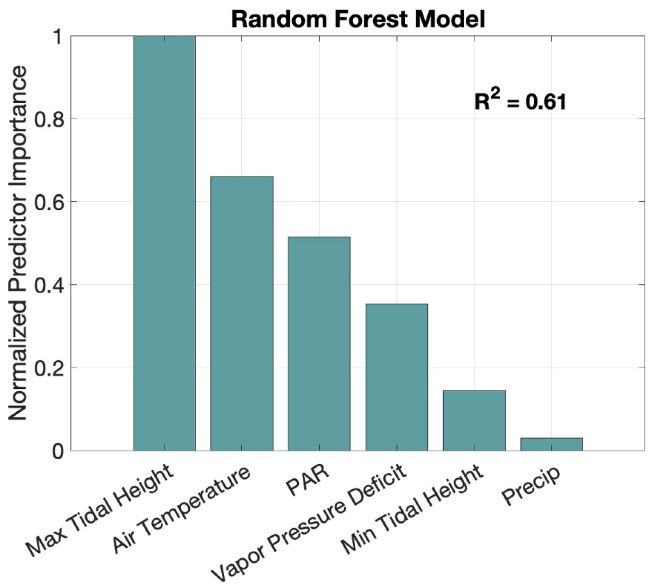

Figure 4. The normalized predictor importance of each random forest input parameter used to model gross primary production's daily depression. The model's R^2 was calculated as the squared correlation between out-of-bag depression data and the model's predicted depression.

soil porewater, making it harder for the plant to pull water up through its roots (Betzen et al., 2019). In response, stomata close to prevent further water loss, which reduces internal CO_2 concentrations and limits photosynthesis. This mechanism may be exacerbated by warmer temperatures and higher VPD in the afternoon, leading to the observed midday depression of GPP. High salinity can also decrease the photosynthetic capacity by increasing plant tissue ion concentrations (DeLaune & Pezeshki, 1994; Maricle, Lee, et al., 2007; Poppe & Rybczyk, 2021). Higher tides can relieve vegetation stress and lead to an increase in photosynthesis, which can explain why midday depression was less severe during periods with higher tides (Jones et al., 2018; Knox et al., 2018; Liu et al., 2020; Nahrawi et al., 2020; Teal, 2001).

In this study, the higher tides and cooler temperatures in 2020 likely contributed to its less severe midday depression of photosynthesis and larger GPP than in other study years. Although 2021 and 2022 were not particularly warm, the reduced tidal flooding led to a decrease in soil moisture, resulting in visible cracking on the marsh soil surface, which likely contributed to the more severe midday depression in these years. While there was the most tidal flooding in 2019, it was also the warmest year and had moderate midday depression of GPP, thus illustrating the opposing effects of tidal flooding and temperature. In the context of climate change, our results highlight the complexity of multiple changing environmental conditions impacting the photosynthesis of salt marshes. Both temperature and sea level will continue to rise in the coming decades. Higher tidal levels may mitigate the severity of midday depression associated with warmer temperatures, but only up to a threshold, beyond which additional flooding becomes a stressor (Huang et al., 2020; Nahrawi et al., 2020).

We acknowledge that the observed skewed diurnal pattern of the NEE flux may not be entirely attributable to a midday depression of GPP. Increases in respiration, driven by rising air temperatures throughout the day, likely also contribute to the afternoon suppression of NEE. Without direct measurements of photosynthesis and respiration from chamber or leaf-level measurements, there is inherent uncertainty in the EC flux partitioning of NEE into GPP and respiration components, making it challenging to attribute the skewed NEE to patterns of photosynthesis or respiration (Lasslop et al., 2010). Nonetheless, previous work in an *S. alterniflora* salt marsh similar to this study found that photosynthesis and respiration measured with a chamber or leaf-level methods reasonably agreed with EC partitioned CO_2 fluxes when the measurement footprints overlapped (Hill & Vargas, 2022). Furthermore, the partitioned respiration flux in this study was within the range of respiration from a salt marsh chamber and leaf-level measurements, as well as other EC-based studies (Hwang & Morris, 1994; Jiang et al., 2009; Mayen et al., 2024). Further, the magnitude of the respiration flux is smaller than the magnitudes of NEE and GPP. Respiration would therefore need to increase by a substantial percentage if it were to drive the observed diurnal pattern of NEE. For example, NEE decreased by 1.6 μmol m^{-2} s^{-1} on average between 10:00 and 14:00 LST in 2021 (Figure 1). Respiration would have to increase by ∼50% in a 4-hr period to account for the change in NEE, excluding concurrent changes in GPP. Given the magnitude of the shift in NEE, decreases in GPP are likely playing a significant role in the diurnal pattern of NEE. Thus, we conclude the partitioned GPP and respiration fluxes are reasonable and that respiration did not contribute to the observed skewed NEE as strongly as GPP.

At longer temporal scales, the persistent midday depression of photosynthesis observed in this study has significant implications for the total salt marsh carbon uptake. We estimated up to an 18% decrease in afternoon photosynthesis compared to the morning across the growing season. Goulden et al. (2004) quantified a similar midday depression of NEE in a tropical rainforest of up to ∼40%, which the authors attributed to a combination of high evaporative demand, high temperature, and intrinsic circadian rhythm. During the 2020 southwest US drought, Y. Zhang et al. (2023) showed grasslands had an average 33% decrease in afternoon light use efficiency compared to the morning. The magnitude of midday depression of GPP is thus not inconsequential and must be

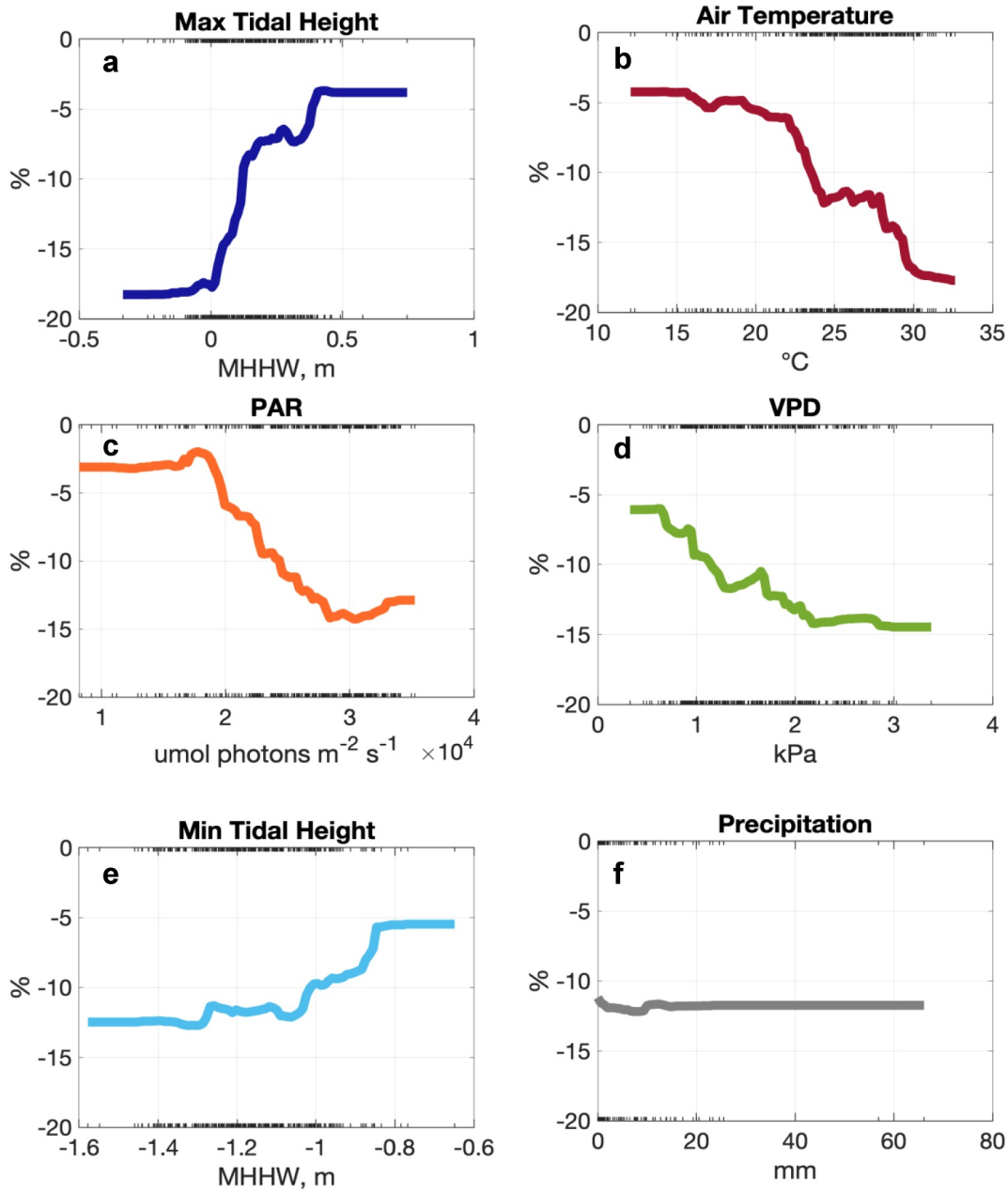

Figure 5. Sensitivity of daily depression of gross primary production to environmental variables in the random forest model. Each panel is a partial dependence plot of the depression's sensitivity to an environmental variable on the *x*-axis. The whiskers on the *x*-axis mark the daily-scale observations of each environmental variable.

carefully interpreted when extrapolating coarser temporal measurements. In contrast to single-overpass polar satellite observations, recent advances in geostationary satellites have made it possible to track diurnal patterns of GPP with greater accuracy and offer a new frontier to continue to examine the midday depression of GPP at larger scales (Khan et al., 2022; X. Li et al., 2021, 2023; Z. Zhang et al., 2023).

Although *S. alterniflora* has Kranz anatomy and ^{13}C:^{12}C ratios typical of C_4 plants, previous studies have shown that it has CO_2 compensation points that fall within the range of C_3 and C_3-C_4 vegetation (Dai & Wiegert, 1997; Kathilankal et al., 2011; Maricle et al., 2009). The tall and short *S. alterniflora* ecophenes are also known to possess significantly different levels of CO_2 uptake and photosynthetic properties that are sensitive to salinity and soil moisture conditions (Giurgevich & Dunn, 1979; Hawman et al., 2024; Shea et al., 1975). This raises the

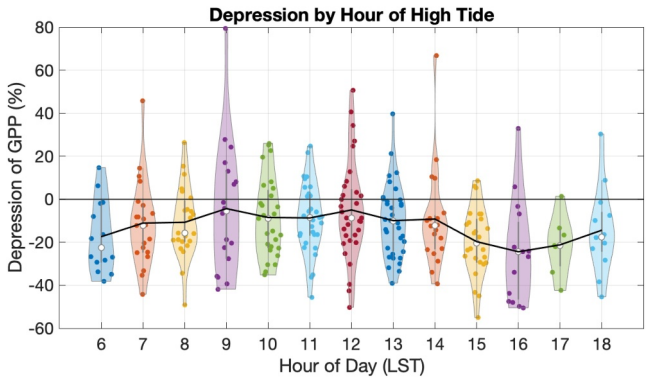

Figure 6. Daily depression of gross primary production (GPP) by the hour of high tide. The colored points within each violin mark individual daily percent depressions on days with a high tide event during the corresponding hour of the day. The white circles are the median depression for each hour of the day. The black line connects the mean depression for each hour of the day. Any points below the horizontal 0% line indicate observations where midday depression of GPP occurs.

possibility that *S. alterniflora* may undergo some level of photorespiration under stressed conditions, which could contribute to the midday decrease in GPP observed in this study. To identify the exact mechanism of midday depression in *S. alterniflora*, future research should include concurrent leaf-level gas exchange measurements within the flux footprint. These data can help conclusively determine whether the reduction in afternoon photosynthesis results from stomatal closure or another process.

5. Conclusions

This study used EC flux observations to measure daily midday depression of photosynthesis and explore the environmental factors influencing the phenomenon in an intertidal salt marsh. We observed ubiquitous midday depression of GPP throughout the 2019–2022 growing seasons, which, to our knowledge, has not been reported in other *S. alterniflora*-dominated marshes. Maximum daily tidal height was the strongest environmental control and attenuated the severity of depression, with higher tide days having less severe depression. Warmer air temperature was also a strong control and contributed to a more severe depression. We suspect that tidal height and air temperature modulate the severity of depression by impacting soil salinity and water availability to plant roots, which ultimately causes stomata to close and reduce CO_2 uptake to minimize water loss in the afternoon. Our results highlight a previously unreported diurnal pattern in a C_4 salt marsh grass that may be further exacerbated by climate change and have significant implications for carbon uptake.

Data Availability Statement

EC flux, tidal, temperature, radiation, and VPD data are available at the VCR-LTER EDI Data Portal via https://doi.org/10.6073/pasta/8796ef2b2b071b8bcfa003fca06b22b7 (Mast & Yang, 2025). The U.S. Climate Reference Network (Cape Charles site) data are available via https://www1.ncdc.noaa.gov/pub/data/uscrn/products/subhourly01/ (NOAA, 2022b). NOAA's Wachapreague tidal station data are available via https://tidesandcurrents.noaa.gov/waterlevels.html?id=8631044 (NOAA, 2022a).

Acknowledgments
This project was supported by funding from the Virginia Coast Reserve Long-Term Ecological Research program (NSF Award 1832221), the Virginia Sea Grant (NOAA Award 724537), and the Virginia Space Grant Consortium. The statements, findings, conclusions, and recommendations are those of the author(s) and do not necessarily reflect the views of Virginia Sea Grant, NOAA, the U.S. Department of Commerce, or the NSF. The authors would like to thank Cora Baird, Tom Burkett, Buck Doughty, Sophia Hoffman, Andrew Jablonski, David Lee, Jonah Morreale, Sally Pusede, Elliott White, and Koong Yi for their support with fieldwork. The authors also thank John Porter for his support with data and site management.

References

Alber, M., Swenson, E. M., Adamowicz, S. C., & Mendelssohn, I. A. (2008). Salt Marsh Dieback: An overview of recent events in the US. *Estuarine, Coastal and Shelf Science*, *80*(1), 1–11. https://doi.org/10.1016/j.ecss.2008.08.009

Betzen, B. M., Smart, C. M., Maricle, K. L., & Maricle, B. R. (2019). Effects of increasing salinity on photosynthesis and plant water potential in Kansas salt marsh species. *Transactions of the Kansas Academy of Science*, *122*(1–2), 49–58. https://doi.org/10.1660/062.122.0105

Biçe, K., Schalles, J., Sheldon, J. E., Alber, M., & Meile, C. (2023). Temporal patterns and causal drivers of aboveground plant biomass in a coastal wetland: Insights from time-series analyses. *Frontiers in Marine Science*, *10*, 1130958. https://doi.org/10.3389/fmars.2023.1130958

Bräutigam, A., & Gowik, U. (2016). Photorespiration connects C_3 and C_4 photosynthesis. *Journal of Experimental Botany*, *67*(10), 2953–2962. https://doi.org/10.1093/jxb/erw056

Charles, H., & Dukes, J. S. (2009). Effects of warming and altered precipitation on plant and nutrient dynamics of a New England salt marsh. *Ecological Applications: A Publication of the Ecological Society of America*, *19*(7), 1758–1773. https://doi.org/10.1890/08-0172.1

Dai, T., & Wiegert, R. G. (1997). A field study of photosynthetic capacity and its response to nitrogen fertilization in *Spartina alterniflora*. *Estuarine, Coastal and Shelf Science*, *45*(2), 273–283. https://doi.org/10.1006/ecss.1996.0175

DeLaune, R. D., & Pezeshki, S. R. (1994). The influence of subsidence and saltwater intrusion on coastal marsh stability: Louisiana Gulf Coast, U. S.A. *Journal of Coastal Research*, 77–89. Retrieved from http://www.jstor.org/stable/25735591

De Leeuw, J., Olff, H., & Bakker, J. P. (1990). Year-to-year variation in salt marsh production as related to inundation and rainfall deficit. *Aquatic Botany*, *36*(2), 139–151. https://doi.org/10.1016/0304-3770(90)90078-y

Diamond, H. J., Karl, T. R., Palecki, M. A., Baker, C. B., Bell, J. E., Leeper, R. D., et al. (2013). U.S. climate reference network after one decade of operations: Status and assessment. *Bulletin America Meteorology Social*, *94*(4), 489–498. https://doi.org/10.1175/BAMS-D-12-00170.1

Duarte, C. M., Losada, I. J., Hendriks, I. E., Mazarrasa, I., & Marbà, N. (2013). The role of coastal plant communities for climate change mitigation and adaptation. *Nature Climate Change*, *3*(11), 961–968. https://doi.org/10.1038/nclimate1970

Dunton, K. H., Hardegree, B., & Whitledge, T. E. (2001). Response of estuarine marsh vegetation to interannual variations in precipitation. *Estuaries*, *24*(6), 851. https://doi.org/10.2307/1353176

Foken, T., Göockede, M., Mauder, M., Mahrt, L., Amiro, B., & Munger, W. (2005). Post-field data quality control. In X. Lee, W. Massman, & B. Law (Eds.), *Handbook of micrometeorology: A guide for surface flux measurement and analysis* (pp. 181–208). Springer. https://doi.org/10.1007/1-4020-2265-4_9

Forbrich, I., Giblin, A. E., & Hopkinson, C. S. (2018). Constraining marsh carbon budgets using long-term C burial and contemporary atmospheric CO_2 fluxes. *Journal of Geophysical Research: Biogeosciences*, *123*(3), 867–878. https://doi.org/10.1002/2017jg004336

Ge, Z. M., Zhang, L. Q., Yuan, L., & Zhang, C. (2014). Effects of salinity on temperature-dependent photosynthetic parameters of a native C_3 and a non-native C_4 marsh grass in the Yangtze Estuary, China. *Photosynthetica*, *52*(4), 484–492. https://doi.org/10.1007/s11099-014-0055-4

Giurgevich, J. R., & Dunn, E. L. (1979). Seasonal patterns of CO_2 and water vapor exchange of the tall and short height forms of *Spartina alterniflora* Loisel in a Georgia salt marsh. *Oecologia*, *43*(2), 139–156. https://doi.org/10.1007/BF00344767

Goulden, M. L., Miller, S. D., Rocha, H. R., Menton, M. C., Freitas, H. C., Silva Figueira, A. M., & Sousa, C. A. D. (2004). Diel and seasonal patterns of tropical forest CO_2 exchange. *Ecological Applications: A Publication of the Ecological Society of America*, *14*, 42–54. https://doi.org/10.1890/02-6008

Griscom, B. W., Adams, J., Ellis, P. W., Houghton, R. A., Lomax, G., Miteva, D. A., et al. (2017). Natural climate solutions. *Proceedings of the National Academy of Sciences of the United States of America*, *114*(44), 11645–11650. https://doi.org/10.1073/pnas.1710465114

Grossiord, C., Buckley, T. N., Cernusak, L. A., Novick, K. A., Poulter, B., Siegwolf, R. T. W., et al. (2020). Plant responses to rising vapor pressure deficit. *New Phytologist*, *226*(6), 1550–1566. https://doi.org/10.1111/nph.16485

Hawman, P. A., Cotten, D. L., & Mishra, D. R. (2024). Canopy heterogeneity and environmental variability drive annual budgets of net ecosystem carbon exchange in a tidal marsh. *Journal of Geophysical Research: Biogeosciences*, *129*(4), e2023JG007866. https://doi.org/10.1029/2023jg007866

Hessini, K., Jeddi, K., Siddique, K. H. M., & Cruz, C. (2021). Drought and salinity: A comparison of their effects on the ammonium-preferring species *Spartina alterniflora*. *Physiologia Plantarum*, *172*(2), 431–440. https://doi.org/10.1111/ppl.13241

Hill, A. C., & Vargas, R. (2022). Methane and carbon dioxide fluxes in a temperate tidal salt marsh: Comparisons between plot and ecosystem measurements. *Journal of Geophysical Research: Biogeosciences*, *127*(7), e2022JG006943. https://doi.org/10.1029/2022jg006943

Huang, Y., Chen, Z., Tian, B., Zhou, C., Wang, J., Ge, Z., & Tang, J. (2020). Tidal effects on ecosystem CO_2 exchange in a *Phragmites* salt marsh of an intertidal shoal. *Agricultural and Forest Meteorology*, *292–293*, 108018. https://doi.org/10.1016/j.agrformet.2020.108108

Hughes, A. L. H., Wilson, A. M., & Morris, J. T. (2012). Hydrologic variability in a salt marsh: Assessing the links between drought and acute marsh dieback. *Estuarine, Coastal and Shelf Science*, *111*, 95–106. https://doi.org/10.1016/j.ecss.2012.06.016

Hwang, Y. H., & Morris, J. T. (1994). Whole-plant gas exchange responses of *Spartina alterniflora* (Poaceae) to a range of constant and transient salinities. *American Journal of Botany*, *81*(6), 659–665. https://doi.org/10.1002/j.1537-2197.1994.tb15500.x

Jiang, L. F., Luo, Y. Q., Chen, J. K., & Li, B. (2009). Ecophysiological characteristics of invasive *Spartina alterniflora* and native species in salt marshes of Yangtze River Estuary, China. *Estuarine, Coastal and Shelf Science*, *81*(1), 74–82. https://doi.org/10.1016/j.ecss.2008.09.018

Jones, S. F., Stagg, C. L., Krauss, K. W., & Hester, M. W. (2018). Flooding alters plant-mediated carbon cycling independently of elevated atmospheric CO_2 concentrations. *Journal of Geophysical Research: Biogeosciences*, *123*(6), 1976–1987. https://doi.org/10.1029/2017jg004369

Kathilankal, J. C., Mozdzer, T. J., Fuentes, J. D., McGlathery, K. J., D'Odorico, P., & Zieman, J. C. (2011). Physiological responses of *Spartina alterniflora* to varying environmental conditions in Virginia marshes. *Hydrobiologia*, *669*(1), 167–181. https://doi.org/10.1007/s10750-011-0681-9

Khan, A. M., Stoy, P. C., Joiner, J., Baldocchi, D., Verfaillie, J., Chen, M., & Otkin, J. A. (2022). The diurnal dynamics of gross primary productivity using observations from the advanced baseline imager on the geostationary operational environmental satellite-R series at an oak Savanna ecosystem. *Journal of Geophysical Research: Biogeosciences*, *127*(3), e2021JG006701. https://doi.org/10.1029/2021jg006701

Kirwan, M. L., Guntenspergen, G. R., & Morris, J. T. (2009). Latitudinal trends in *Spartina alterniflora* productivity and the response of coastal marshes to global change. *Global Change Biology*, *15*(8), 1982–1989. https://doi.org/10.1111/j.1365-2486.2008.01834.x

Knox, S. H., Windham-Myers, L., Anderson, F., Sturtevant, C., & Bergamaschi, B. (2018). Direct and indirect effects of tides on ecosystem-scale CO_2 exchange in a brackish tidal marsh in Northern California. *Journal of Geophysical Research: Biogeosciences*, *123*(3), 787–806. https://doi.org/10.1002/2017jg004048

Lamers, L. P. M., Govers, L. L., Janssen, I. C. J. M., Geurts, J. J. M., Van der Welle, M. E. W., Van Katwijk, M. M., et al. (2013). Sulfide as a soil phytotoxin-a review. *Frontiers in Plant Science*, *4*, 268. https://doi.org/10.3389/fpls.2013.00268

Lara, M. V., & Andreo, C. S. (2011). C4 plants adaptation to high levels of CO_2 and to drought environments. In *Abiotic stress in plants-mechanisms and adaptations* (pp. 415–428).

Lasslop, G., Reichstein, M., Papale, D., Richardson, A. D., Arneth, A., Barr, A., et al. (2010). Separation of net ecosystem exchange into assimilation and respiration using a light response curve approach: Critical issues and global evaluation. *Global Change Biology*, *16*(1), 187–208. https://doi.org/10.1111/j.1365-2486.2009.02041.x

Li, H., Wang, C., Yu, Q., & Smith, E. (2022). Spatiotemporal assessment of potential drivers of salt marsh dieback in the North inlet-Winyah Bay estuary, South Carolina (1990-2019). *Journal of Environmental Management*, *313*, 114907. https://doi.org/10.1016/j.jenvman.2022.114907

Li, X., Ryu, Y., Xiao, J., Dechant, B., Liu, J., Li, B., et al. (2023). New-generation geostationary satellite reveals widespread midday depression in dryland photosynthesis during 2020 western U.S. heatwave. *Science Advances*, *9*(31), eadi0775. https://doi.org/10.1126/sciadv.adi0775

Li, X., Xiao, J., Fisher, J. B., & Baldocchi, D. D. (2021). ECOSTRESS estimates gross primary production with fine spatial resolution for different times of day from the International Space Station. *Remote Sensing of Environment*, *258*, 112360. https://doi.org/10.1016/j.rse.2021.112360

LI-COR. (2020). *EddyPro software instruction manual* (Vol. 7). LI-COR Inc.

Lin, C., Gentine, P., Frankenberg, C., Zhou, S., Kennedy, D., & Li, X. (2019). Evaluation and mechanism exploration of the diurnal hysteresis of ecosystem fluxes. *Agricultural and Forest Meteorology*, *278*, 107642. https://doi.org/10.1016/j.agrformet.2019.107642

Liu, Z., Fagherazzi, S., She, X., Ma, X., Xie, C., & Cui, B. (2020). Efficient tidal channel networks alleviate the drought-induced die-off of salt marshes: Implications for coastal restoration and management. *The Science of the Total Environment*, *749*, 141493. https://doi.org/10.1016/j.scitotenv.2020.141493

Lovelock, C. E., & Reef, R. (2020). Variable impacts of climate change on blue carbon. *One Earth*, *3*(2), 195–211. https://doi.org/10.1016/j.oneear.2020.07.010

Maricle, B. R., Cobos, D. R., & Campbell, C. S. (2007). Biophysical and morphological leaf adaptations to drought and salinity in salt marsh grasses. *Environmental and Experimental Botany*, *60*(3), 458–467. https://doi.org/10.1016/j.envexpbot.2007.01.001

Maricle, B. R., Koteyeva, N. K., Voznesenskaya, E. V., Thomasson, J. R., & Edwards, G. E. (2009). Diversity in leaf anatomy, and stomatal distribution and conductance, between salt marsh and freshwater species in the C_4 genus *Spartina* (Poaceae). *New Phytologist*, *184*(1), 216–233. https://doi.org/10.1111/j.1469-8137.2009.02903.x

Maricle, B. R., & Lee, R. W. (2006). Effects of environmental salinity on carbon isotope discrimination and stomatal conductance in Spartina grasses. *Marine Ecology Progress Series*, *313*, 305–310. https://doi.org/10.3354/meps313305

Maricle, B. R., Lee, R. W., Hellquist, C. E., Kiirats, O., & Edwards, G. E. (2007). Effects of salinity on chlorophyll fluorescence and CO_2 fixation in C_4 estuarine grasses. *Photosynthetica*, *45*(3), 433–440. https://doi.org/10.1007/s11099-007-0072-7

Mast, H., & Yang, X. (2025). *VCR fowling point salt marsh flux tower, 2019-2023 ver 5*. Environmental Data Initiative. https://doi.org/10.6073/pasta/8796ef2b2b071b8bcfa003fca06b22b7

MATLAB. (2022). *The MathWorks Inc. (2022). MATLAB version: 9.13.0 (R2022b), Natick, Massachusetts*. The MathWorks Inc. Retrieved from https://www.mathworks.com

Mayen, J., Polsenaere, P., Lamaud, E., Arnaud, M., Kostyrka, P., Bonnefond, J., et al. (2024). Atmospheric CO_2 exchanges measured by Eddy covariance over a temperate salt marsh and influence of environmental controlling factors. *Biogeosciences*, *21*(4), 993–1016. https://doi.org/10.5194/bg-21-993-2024

McKee, K. L., Mendelssohn, I. A., & Materne, M. D. (2004). Acute salt marsh dieback in the Mississippi River deltaic plain: A drought-induce phenomenon? *Global Ecology and Biogeography*, *13*, 65–74. https://doi.org/10.1111/j.1466-882X.2004.00075.x

Mcleod, E., Chmura, G. L., Bouillon, S., Salm, R., Björk, M., Duarte, C. M., et al. (2011). A blueprint for blue carbon: Toward an improved understanding of the role of vegetated coastal habitats in sequestering CO_2. https://doi.org/10.1890/110004

Moncrieff, J. B., Clement, R., Finnigan, J., & Meyers, T. (2005). Averaging, detrending, and filtering of eddy covariance time series. In X. Lee, W. Massman, & B. Law (Eds.), *Handbook of micrometeorology: A guide for surface flux measurement and analysis* (pp. 7–31). Springer. https://doi.org/10.1007/1-4020-2265-4_2

Moncrieff, J. B., Massheder, J. M., de Bruin, H., Elbers, J., Friborg, T., Heusinkveld, B., et al. (1997). A system to measure surface fluxes of momentum, sensible heat, water vapour and carbon dioxide. *Journal of Hydrology*, *188–189*, 589–611. https://doi.org/10.1016/S0022-1694(96)03194-0

Nahrawi, H., Leclerc, M. Y., Pennings, S., Zhang, G., Singh, N., & Pahari, R. (2020). Impact of tidal inundation on the net ecosystem exchange in daytime conditions in a salt marsh. *Agricultural and Forest Meteorology*, *294*, 108133. https://doi.org/10.1016/j.agrformet.2020.108133

National Oceanic and Atmospheric Administration. (2022a). Center for operational oceanographic products and services (CO-OPS) [Dataset]. *Tides and Currents*. Retrieved from https://tidesandcurrents.noaa.gov/waterlevels.html?id=8631044

National Oceanic and Atmospheric Administration. (2022b). National centers for environmental information: U.S. climate reference network [Dataset]. *Cape Charles*. Retrieved from https://www1.ncdc.noaa.gov/pub/data/uscrn/products/subhourly01/

Nellemann, C., & Corcoran, E. (2009). *Blue carbon: The role of healthy oceans in binding carbon: A rapid response assessment*. UNEP/Earthprint.

O'Donnell, K. L., Bernhardt, E. S., Yang, X., Emanuel, R. E., Ardón, M., Lerdau, M. T., et al. (2024). Saltwater intrusion and sea level rise threatens U.S. rural coastal landscapes and communities. *Anthropocene*, *45*, 100427. https://doi.org/10.1016/j.ancene.2024.100427

Odum, W. E. (1988). Comparative ecology of tidal freshwater and salt marshes. *Annual Review of Ecology and Systematics*, *19*(1), 147–176. https://doi.org/10.1146/annurev.es.19.110188.001051

Papale, D., Reichstein, M., Aubinet, M., Canfora, E., Bernhofer, C., Kutsch, W., et al. (2006). Towards a standardized processing of net ecosystem exchange measured with eddy covariance technique: Algorithms and uncertainty estimation. *Biogeosciences*, *3*(4), 571–583. https://doi.org/10.5194/bg-3-571-2006

Pardo, J., & VanBuren, R. (2021). Evolutionary innovations driving abiotic stress tolerance in C_4 grasses and cereals. *The Plant Cell*, *33*(11), 3391–3401. https://doi.org/10.1093/plcell/koab205

Pastorello, G., Trotta, C., Canfora, E., Chu, H., Christianson, D., Cheah, Y.-W., et al. (2020). The FLUXNET2015 dataset and the ONEFlux processing pipeline for eddy covariance data. *Scientific Data*, *7*(1), 225. https://doi.org/10.1038/s41597-020-0534-3

Paul-Limoges, E., Damm, A., Hueni, A., Liebisch, F., Eugster, W., Schaepman, M. E., & Buchmann, N. (2018). Effect of environmental conditions on sun-induced fluorescence in a mixed forest and a cropland. *Remote Sensing of Environment*, *219*, 310–323. https://doi.org/10.1016/j.rse.2018.10.018

Pearcy, R. W., & Ustin, S. L. (1984). Effects of salinity on growth and photosynthesis of three California tidal marsh species. *Oecologia*, *62*(1), 68–73. https://doi.org/10.1007/BF00377375

Peterson, P. M., Romaschenko, K., Arrieta, Y. H., & Saarela, J. M. (2014a). (2332) Proposal to conserve the name *sporobolus* against *Spartina, Crypsis, Ponceletia*, and *Heleochloa* (*Poaceae: Chloridoideae: Sporobolinae*). *Taxon*, *63*(6), 1373–1374. https://doi.org/10.12705/636.23

Peterson, P. M., Romaschenko, K., Arrieta, Y. H., & Saarela, J. M. (2014b). A molecular phylogeny and new subgeneric classification of *Sporobolus* (Poaceae: Chloridoideae: Sporobolinae). *Taxon*, *63*(6), 1212–1243. https://doi.org/10.12705/636.19

Poppe, K. L., & Rybczyk, J. M. (2021). Climatic impacts on salt marsh vegetation. In *Salt marshes: Function, dynamics, and stresses* (pp. 337–366). Cambridge University Press. https://doi.org/10.1017/9781316888933.016

Qiu, B., Ge, J., Guo, W., Pitman, A. J., & Mu, M. (2020). Responses of Australian dryland vegetation to the 2019 heat wave at a subdaily scale. *Geophysical Research Letters*, *47*(4), e2019GL086569. https://doi.org/10.1029/2019GL086569

Reichstein, M., Falge, E., Baldocchi, D., Papale, D., Aubinet, M., Berbigier, P., et al. (2005). On the separation of net ecosystem exchange into assimilation and ecosystem respiration: Review and improved algorithm. *Global Change Biology*, *11*(9), 1424–1439. https://doi.org/10.1111/j.1365-2486.2005.001002.x

Rolando, J. L., Hodges, M., Garcia, K. D., Krueger, G., Williams, N., Carr, J., Jr., et al. (2023). Restoration and resilience to sea level rise of a salt marsh affected by dieback events. *Ecosphere*, *14*(4), e4467. https://doi.org/10.1002/ecs2.4467

Rosentreter, J. A., Laruelle, G. G., Bange, H. W., Bianchi, T. S., Busecke, J. J. M., Cai, W.-J., et al. (2023). Coastal vegetation and estuaries are collectively a greenhouse gas sink. *Nature Climate Change*, *13*(6), 579–587. https://doi.org/10.1038/s41558-023-01682-9

Russell, S. J., Windham-Myers, L., Stuart-Haentjens, E. J., Bergamaschi, B. A., Anderson, F., Oikawa, P., & Knox, S. H. (2023). Increased salinity decreases annual gross primary productivity at a Northern California brackish tidal marsh. *Environmental Research Letters*, *18*(3), 034045. https://doi.org/10.1088/1748-9326/acbbdf

Shea, M. L., Warren, R. S., & Niering, W. A. (1975). Biochemical and transplantation studies of the growth form of *Spartina alterniflora* on Connecticut salt marshes. *Ecology*, *56*(2), 461–466. https://doi.org/10.2307/1934977

Shen, C., Zhang, C., Xin, P., Kong, J., & Li, L. (2018). Salt dynamics in coastal marshes: Formation of hypersaline zones. *Water Resources Research*, *54*(5), 3259–3276. https://doi.org/10.1029/2017WR022021

Stagg, C. L., Osland, M. J., Moon, J. A., Feher, L. C., Laurenzano, C., Lane, T. C., et al. (2021). Extreme precipitation and flooding contribute to sudden vegetation dieback in a coastal salt marsh. *Plants*, *10*(9), 1841. https://doi.org/10.3390/plants10091841

Teal, J. M. (2001). Salt marshes and mud flats. In J. H. Steele (Ed.), *Encyclopedia of ocean sciences* (pp. 2490–2495). Academic Press. https://doi.org/10.1006/rwos.2001.0087

Vickers, D., & Mahrt, L. (1997). Quality control and flux sampling problems for tower and aircraft data. *Journal of Atmospheric and Oceanic Technology*, *14*(3), 512–526. https://doi.org/10.1175/1520-0426(1997)014<0512:QCAFSP>2.0.CO;2

Webb, E. K., Pearman, G. I., & Leuning, R. (1980). Correction of flux measurements for density effects due to heat and water vapour transfer. *Quarterly Journal of the Royal Meteorological Society*, *106*(447), 85–100. https://doi.org/10.1002/qj.49710644707

Więski, K., & Pennings, S. C. (2014). Climate drivers of *Spartina alterniflora* saltmarsh production in Georgia, USA. *Ecosystems*, *17*(3), 473–484. https://doi.org/10.1007/s10021-013-9732-6

Wilczak, J. M., Oncley, S. P., & Stage, S. A. (2001). Sonic anemometer tilt correction algorithms. *Boundary-Layer Meteorology*, *99*(1), 127–150. https://doi.org/10.1023/A:1018966204465

Wilson, K. B., Baldocci, D., Falge, E., Aubinet, M., Berbigier, P., Bernhofer, C., et al. (2003). Diurnal centroid of ecosystem energy and carbon fluxes at FLUXNET sites. *Journal of Geophysical Research*, *108*(D21), 4664. https://doi.org/10.1029/2001JD001349

Wutzler, T., Lucas-Moffat, A., Migliavacca, M., Knauer, J., Sickel, K., Šigut, L., et al. (2018). Basic and extensible post-processing of eddy covariance flux data with REddyProc. *Biogeosciences*, *15*(16), 5015–5030. https://doi.org/10.5194/bg-15-5015-2018

Xin, P., Li, L., & Barry, D. A. (2013). Tidal influence on soil conditions in an intertidal creek-marsh system. *Water Resources Research*, *49*(1), 137–150. https://doi.org/10.1029/2012wr012290

Xin, P., Zhou, T., Lu, C., Shen, C., Zhang, C., D'Alpaos, A., & Li, L. (2017). Combined effects of tides, evaporation and rainfall on the soil conditions in an intertidal creek-marsh system. *Advances in Water Resources*, *103*, 1–15. https://doi.org/10.1016/j.advwatres.2017.02.014

Xu, D. Q., & Shen, Y. K. (1996). Midday depression of photosynthesis. In *Handbook of photosynthesis* (pp. 451–459).

Xu, H., Xiao, J., & Zhang, Z. (2020). Heatwave effects on gross primary production of northern mid-latitude ecosystems. *Environmental Research Letters*, *15*(7), 074027. https://doi.org/10.1088/1748-9326/ab8760

Xu, X., Xin, P., & Yu, X. (2024). Interactions of macropores with tides, evaporation and rainfall and their effects on pore-water salinity in salt marshes. *Journal of Hydrology*, *630*, 130740. https://doi.org/10.1016/j.jhydrol.2024.130740

Zhang, Y., Fang, J., Smith, W. K., Wang, X., Gentine, P., Russell, S., et al. (2023). Satellite solar-induced chlorophyll fluorescence tracks physiological drought stress development during 2020 southwest US drought. *Global Change Biology*, *29*(12), 3395–3408. https://doi.org/10.1111/gcb.16683

Zhang, Z., Cescatti, A., Wang, Y. P., Gentine, P., Xiao, J., Guanter, L., et al. (2023). Large diurnal compensatory effects mitigate the response of Amazonian forests to atmospheric warming and drying. *Science Advances*, *9*(21), eabq4974. https://doi.org/10.1126/sciadv.abq4974